

# ChinaRiceCalendar-Seasonal Crop Calendars for Early, Middle, and Late Rice in China

Hui Li<sup>1</sup>, Xiaobo Wang<sup>2,\*</sup>, Shaoqiang Wang<sup>1,2,3,4,\*</sup>, Jinyuan Liu<sup>1</sup>, Yuanyuan Liu<sup>2</sup>, Zhenhai Liu<sup>2</sup>, Shiliang Chen<sup>1,2</sup>, Qinyi Wang<sup>1</sup>, Tongtong Zhu<sup>1</sup>, Lunche Wang<sup>1</sup>, Lizhe Wang<sup>5</sup>

<sup>1</sup>Key Laboratory of Regional Ecology and Environmental Change, School of Geography and Information Engineering, China University of Geosciences, Wuhan, 430074, China

<sup>2</sup>Key Laboratory of Ecosystem Network Observation and Modeling, Institute of Geographic Sciences and Natural Resources Research, CAS, Beijing, 100101, China

<sup>3</sup>State Key Laboratory of Biogeology and Environmental Geology, China University of Geosciences, Wuhan 430074, China;

<sup>4</sup>College of Resources and Environment, University of Chinese Academy of Sciences, Beijing 100049, China;

<sup>5</sup>Hubei Key Laboratory of Intelligent Geo-Information Processing, China University of Geosciences, Wuhan 430074, China

\*Correspondence to: Xiaobo Wang (wxbwxb1995@163.com); Shaoqiang Wang (sqwang@igsnr.ac.cn)

**Abstract.** Long-time series and large-scale rice calendar datasets provide valuable information for agricultural planning and field management in rice-based cropping systems. However, current regional-level rice calendar datasets do not accurately distinguish between rice seasons in China, causing uncertainty in crop model simulation and climate change impact analysis. Based on satellite remote sensing data, we extracted transplanting, heading, and maturity dates of early-, middle-, and late-season rice across China from 2003 to 2022, and established a multi-season rice calendar dataset named ChinaRiceCalendar. Overall, the ChinaRiceCalendar dataset shows a good agreement with field-observed phenological dates of early, middle, and late rice in Chinese Agricultural Meteorological Stations (AMSs). According to the calendar data from 2003 to 2022 in China, the transplanting dates for early, middle, and late rice shifted by +0.7, -0.7, and -5.1 DOY/decade, respectively; the heading date for early, middle, and late rice shifted by -0.5, +2.7, and -0.6 DOY/decade, respectively; the maturity date for early, middle, and late rice shifted by -0.7, +3.8, and -1.6 DOY/decade, respectively. The ChinaRiceCalendar can be utilized to investigate and optimize the spatio-temporal structure of rice cultivation in China under climate and land-use change.

## 1 Introduction

As one of the major food crops, rice feeds nearly half of the world's population (Nelson and Gumma, 2015; Fahad et al., 2019). In the context of climate change, continued warming is projected to result in shorter crop growth periods, lower rice productivity, and food insecurity in the Asian monsoon region

36 (Carleton, 2017; Zhao et al., 2017; IPCC, 2022). Revealing changes in rice phenology will facilitate  
37 timely adjustment of planting time, rice cultivars, and cropping systems under global warming (Waha  
38 et al., 2013; Wang et al., 2022; Wang et al., 2024). Moreover, a dynamic rice calendar with key  
39 phenological dates is integral to agricultural monitoring and farmer support systems (Laborte et al.,  
40 2017; Fritz et al., 2019; Mishra et al., 2021). Large-scale rice calendars can contribute to more reliable  
41 simulations of crop growth and yield at regional and global scales (Franke et al., 2020).

42  
43 Satellite remote sensing is an effective tool for detecting long-term trends in crop phenology at the  
44 regional scale (Xiao et al., 2006; Kotsuki and Tanaka, 2015; Luo et al., 2020; Gao and Zhang, 2021;  
45 Mishra et al., 2021). Crop phenology detection methods based on remote sensing vegetation indices  
46 (VIs) can be categorized into threshold, inflection point, and shape model approaches. The threshold  
47 approaches assume that a development stage begins when the VI value exceeds a predefined threshold  
48 (Jönsson et al., 2004; Boschetti et al., 2009; Pan et al., 2015; Guo et al., 2016). The inflection point  
49 approaches reconstruct the VI time-series curve by filter smoothing or function fitting, and then  
50 corresponds the maxima, minima, and inflection points on the curve to the key phenological events  
51 (Zhang et al., 2003; Sakamoto et al., 2005; Sun et al., 2009; Wang et al., 2019). The shape model  
52 approaches fit observed VI time-series curves by geometric scaling a robust standard VI time-series  
53 curve for the specific crop to identify development stages (Sakamoto et al., 2010; More et al., 2016;  
54 Zeng et al., 2016; Sakamoto et al., 2018). In addition to the methods based on time series of VIs, there  
55 are also rule-based algorithms that integrate multiple approaches and indicators to detect crop  
56 phenology, such as the PhenoRice algorithm proposed by Boschetti et al. (2017). The PhenoRice  
57 algorithm, which combines the advantages of threshold and inflection point approaches, utilizes the  
58 Enhanced Vegetation Index (EVI), the Normalized Difference Flood Index (NDFI), and the land  
59 surface temperature (LST) to estimate rice planting dates. The PhenoRice algorithm excels at  
60 extracting rice phenology in multiple cropping systems and has been widely used in East Asia, South  
61 Asia, Southeast Asia, and Europe (Busetto et al., 2019; Liu et al., 2020; Mishra et al., 2021). However,  
62 the performance of the PhenoRice algorithm depends on the division of rice seasons, which requires  
63 expert knowledge about rice-based cropping systems in different regions (Mishra et al., 2021).

64  
65 In China, there are at least three rice-growing seasons (early, middle, and late seasons) in diverse  
66 rice-based cropping systems (e.g., single-rice, double-rice, rice-wheat, rice-rapeseed, and  
67 rice-vegetable systems) (Frolking et al., 2002; Qiu et al., 2003; Cao et al., 2021; He et al., 2021).  
68 Generally, early, middle, and late-season rice in China are transplanted around Day Of Year (DOY)  
69 80-130, DOY 130-180, and DOY 180-230, respectively. Their typical maturity dates align with DOY  
70 160-220, DOY 240-290, and DOY 270-330, respectively. Although field observations are important  
71 data sources for studying rice calendars in different growing seasons, they are usually limited by spatial  
72 and temporal discontinuities (Zhao et al., 2016; Wang et al., 2017). Therefore, previous studies have  
73 typically utilized satellite remote sensing products to establish rice calendar datasets at the regional  
74 scale (Shihua et al., 2014; Liu et al., 2019; Bai and Xiao, 2020; Luo et al., 2020; Mishra et al., 2021).  
75 Nevertheless, these calendar datasets based on satellite remote sensing do not rationally classify rice  
76 growing seasons across China. For example, the dataset ChinaCropPhen1km only distinguishes  
77 between early and late rice in double-rice systems (Luo et al., 2020); the assumptions of the dataset  
78 RICA about rice heading dates in different seasons do not correspond to the realities in China (Mishra  
79 et al., 2021); Shen et al. (2023) produced high-resolution distribution maps of single-season rice but did

80 not explore multiple rice cropping systems. Early-, middle- and late-season rice in China are not only  
81 planted at different times, but also have distinguishing varietal characteristics, such as different  
82 temperature and photoperiod sensitivities (Zong et al., 2021). Thus, a crop calendar that accurately  
83 classifies rice seasons will provide reliable data for agricultural models to calibrate crop parameters at  
84 the variety level. Moreover, effective identification of different rice seasons will help analyze the  
85 response and adaptation of rice phenology to climate change.

86

87 Therefore, to address the shortcomings of the existing rice calendar datasets in China, we attempted to  
88 improve the PhenoRice algorithm and use satellite remote sensing data to (1) establish crop calendars  
89 for early, middle, and late rice in China; (2) validate the extracted rice calendars in different growing  
90 seasons; and (3) explore the spatio-temporal changes of rice calendar dates in major agricultural zones  
91 across China from 2003 to 2022.

## 92 **2 Data and Methodology**

### 93 **2.1 Study area**

94 We selected seven agricultural zones in China as the study area: the Northeast Plain (NP),  
95 Huanghuaihai Plain (HP), Loess Plateau (LP), Middle and Lower Yangtze River Region (MLY), South  
96 China Region (SC), Yunnan-Guizhou Plateau (YGP), and Sichuan Basin and Surrounding Region  
97 (SCS) (Fig. 1). Due to limited hydrothermal resources, the NP and HP zones mainly cultivate  
98 single-season rice. Early, middle, and late rice exist in different cropping systems in the MLY zone.  
99 The SC zone has a higher cropping frequency than other zones and usually cultivates rice twice a year.  
100 Parts of Hainan Province cultivate rice three times a year. Agricultural zoning data were obtained  
101 from Resources and Environment Science and Data Center  
102 (<https://www.resdc.cn/data.aspx?DATAID=275>).

### 103 **2.2 Data**

#### 104 **2.2.1 Satellite Imagery**

105 MODIS (Moderate Resolution Imaging Spectroradiometer) remote sensing data are widely used in  
106 crop phenology detection because of their excellent performance in temporal and spatial continuity  
107 (Reed et al., 1994; Zhang et al., 2003; Zhao et al., 2011; Son et al., 2013). We selected two MODIS  
108 EVI products for the study area during 2003–2022: MOD13Q1 (TERRA data) and MYD13Q1 (AQUA  
109 data) (<https://doi.org/10.5067/MODIS/MOD13Q1.061>). Because the TERRA and AQUA data are  
110 based on the synthetic period of moving eight days from each other, the time series of the two 16-day  
111 products of MOD13Q1 and MYD13Q1 have a temporal resolution of 8 days (Boschetti et al., 2017).  
112 The red ( $\rho_{RED}$ ) and near-red ( $\rho_{SWIR}$ ) bands of MOD13Q1 and MYD13Q1 were used to calculate the  
113 Normalized Flooding Index (NDFI) (Eq. 1). The Pixel Reliability, Usefulness Index, and Blue Band  
114 Reflectance from MOD13Q1/MYD13Q1 were used to assess data quality. The Land Surface  
115 Temperature (LST) product MOD11A2 (<https://doi.org/10.5067/MODIS/MOD11A2.061>) were  
116 employed to estimate land surface temperature during rice planting.

117 
$$NDFI = \frac{\rho_{RED} - \rho_{SWIR}}{\rho_{RED} + \rho_{SWIR}} \quad (1)$$

118 All above raster data were downloaded and spatially aggregated to 1km resolution by the Google Earth  
119 Engine (GEE) platform and the Python package of Geemap (Wu, 2020).

### 120 2.2.2 Validation Data

121 We collected field observations including transplanting, heading, and maturity dates of early, middle  
122 (single-season), and late rice between 2003 and 2013 from 338 Agricultural Meteorological Stations  
123 (AMSS, <https://data.cma.cn/>) in China. Moreover, we compared ChinaRiceCalendar with other  
124 multi-season and regional-scale calendar datasets, including the RiceAtlas dataset based on the  
125 agricultural statistics (Laborte et al., 2017), the ChinaCropPhen1km dataset based on the Global Land  
126 Surface Satellite (GLASS) leaf area index (LAI) products (Luo et al., 2020), and the RICA dataset  
127 based on the MOD13Q1/MYD13Q1 products (Mishra et al., 2021).

### 128 2.2.3 Additional Data

129 Cropland data were obtained from the International Geosphere-Biosphere Program (IGBP)  
130 classification of the MODIS land cover product (MCD12Q1) from 2003 to 2022  
131 (<https://doi.org/10.5067/MODIS/MCD12Q1.006>). Digital elevation model (DEM) data used to create a  
132 terrain mask were obtained from the Shuttle Radar Topography Mission (SRTM,  
133 <https://srtm.csi.cgiar.org>). Both data are resampled to a spatial resolution of 1 km.

## 134 2.3 Methodology

135 The technology roadmap of this study is shown in Fig. 2.

### 136 2.3.1 Data pre-processing

137 The data pre-processing in the study falls into three steps:

138

- 139 1. The signal of agronomic flooding was used to help identify the rice transplanting period, but  
140 non-agricultural wetlands may have similar flooding signals to paddy fields (Dong and Xiao,  
141 2016; Han et al., 2022). Thus, the annual cropland extent from 2003 to 2020 was used to establish  
142 a cropland mask to screen the cropland pixels of the MODIS EVI data.
- 143 2. Given that too high an elevation or too great a slope is unsuitable for paddy rice cultivation  
144 (Gumma et al., 2011; Dong and Xiao, 2016), only the image pixels with an elevation below 2600  
145 m and a slope less than 8° were selected to extract rice calendars (Han et al., 2022).
- 146 3. To reduce the impacts of cloud contamination, we deleted the image pixels with reflectance  
147 greater than 0.2 in the blue band (Xiao et al., 2006).

### 148 2.3.2 Estimation of rice area and cropping calendar

149 We combined the PhenoRice algorithm (Boschetti et al., 2017) with a growing season division method  
150 (Kong et al., 2022) to extract rice pixels and cropping calendars in different growing seasons. Firstly,

151 we identified possible crop heading periods based on a weighted-smoothed EVI time-series curve in  
152 each image pixel. Then we input the possible heading periods into the PhenoRice algorithm to divide  
153 potential growing seasons and check if the corresponding EVI time series belongs to rice. Lastly, we  
154 estimated rice planting, heading, and maturity dates and categorized them into early-, middle-, and  
155 late-season calendars according to the respective transplanting and maturity times.

156 ① **Divide potential growing seasons:** The PhenoRice algorithm requires a pre-specification of rice  
157 heading periods in different growing seasons to extract the corresponding VI time series. To  
158 reduce the uncertainty caused by the artificial division of growing seasons, we employed the  
159 *phenofit* R package developed by Kong et al. (2022) to identify possible heading periods in each  
160 image pixel. 1) The weighted Whittaker method in the *phenofit* R package was employed to  
161 smooth the MODIS-EVI time series (Kong et al., 2022). The Whittaker smoothing function can  
162 robustly capture seasonal signals with little noise interference, and it is widely used to identify  
163 crop phenology (Atzberger and Eilers, 2011; Bush et al., 2017). The curve fitting mainly relies on  
164 information from good-quality points, but also extracts the limited information available from the  
165 marginal- and bad-quality points. During the rough fitting to the EVI time series, we categorized  
166 the data quality of the observations according to their Quality Control (QC) information  
167 (SummaryQA of MOD13A1) and assigned weights of 1.0, 0.5, and 0.2 to the good-, marginal-,  
168 and bad-quality VI observations, respectively. 2) Following Kong et al. (2022), the possible  
169 heading date (peak point date) in each crop season was identified by the smoothed EVI time series,  
170 based on the rules that only one peak value is inside a growing season and two trough values  
171 define a growing season. 3) The possible heading periods (peak point dates  $\pm 16$  days) detected in  
172 each image pixel were input into the PhenoRice algorithm to generate the potential growing  
173 seasons.

174 ② **Check if the pixel belongs to a rice-cultivated area:** Whether the pixel belongs to a rice  
175 cultivated area during the selected growing season is checked using the following procedure  
176 (Boschetti et al., 2017): 1) Compare the observed maximum, and minimum EVI values with the  
177 corresponding thresholds for paddy fields ( $EVI_{max\_th}$ , and  $EVI_{min\_th}$ ) to reduce misclassification  
178 problems with evergreen forests and non-vegetative areas; 2) Check for the existence of a  
179 maximum inflection point on the EVI curve, which must show a consistent increasing trend  
180 before the maxima and a consistent decreasing trend after the maxima. The time interval between  
181 the inflection points of the minimum and maximum EVI values during the season must fall within  
182 the range of rice vegetative growing periods [ $v11$ ,  $v12$ ]; 3) Check if the meteorological conditions  
183 on the day of the minimum are favourable for rice crop establishment based on a MODIS-LST  
184 value above a specified threshold ( $LST_{th}$ ); 4) Detect a flood signal ( $NDFI \geq minndfi$ ) within a time  
185 window ( $winfl$ ) centred on the minimum; 5) Check if there is a consistent increase in EVI  
186 observed after the minimum; 6) Check if EVI decreases by more than  $decrth\%$  of the amplitude of  
187 the min-max range in a time window after the maxima ( $windecr$ ). Only if all the above  
188 requirements are satisfied, the selected growing season in the pixel is labelled as a rice season.  
189 The PhenoRice parameters used in the study were calibrated by the phenological observations  
190 from the AMSs in China (Table 1).

191 ③ **Estimate rice planting, heading, and maturity dates:** The rice calendar dates were estimated in  
192 the detected rice pixels within the rice seasons. On the EVI time-series curve, the onset date of the

193 field growth period corresponds to the date of the minimum point closest to the retained  
 194 maximum; the heading time corresponds to the date of the retained maximum point; the maturity  
 195 date corresponds to the date when the EVI declined by *decrth%* of the amplitude of the min-max  
 196 range. Additionally, the study categorized the detected rice calendars into early, middle, and late  
 197 seasons based on their respective range of transplanting and maturity dates in each province  
 198 (Table 2).

### 199 2.3.3 Data validation

200 Taking AMS field observations as benchmarks, we evaluated the accuracy of rice calendar dates  
 201 derived from four multi-season rice calendars: ChinaRiceCalendar, ChinaCropPhen1km, RiceAtlas,  
 202 and RICA. These regional rice calendars can be divided into 2 categories: raster datasets  
 203 (ChinaRiceCalendar and ChinaCropPhen1km) and district-level datasets (RiceAtlas and RICA). For  
 204 ChinaRiceCalendar and ChinaCropPhen1km, we sought the nearest rice pixel around each AMS site  
 205 for data pairing. In instances where there was no corresponding rice pixel within a 4 km radius around  
 206 an AMS site, the site was excluded from the analysis. Also, we conducted a comparison between  
 207 district-level rice calendars obtained from RiceAtlas and RICA, juxtaposed with AMS data distributed  
 208 within the respective districts. Two criteria were used to evaluate the accuracy of the estimated rice  
 209 areas and cropping dates in each season, namely Root Mean Squared Error (RMSE, Eq. (2)) and R<sup>2</sup> (Eq.  
 210 (3)):

$$211 \quad \text{RMSE} = \sqrt{\frac{1}{N} \sum_{i=1}^N (\text{true}_i - \text{est}_i)^2} \quad (2)$$

$$212 \quad R^2 = \left( \frac{\sum_{i=1}^N (\text{est}_i - \overline{\text{est}})(\text{true}_i - \overline{\text{true}})}{\sqrt{\sum_{i=1}^N (\text{est}_i - \overline{\text{est}})^2} \sqrt{\sum_{i=1}^N (\text{true}_i - \overline{\text{true}})^2}} \right)^2 \quad (3)$$

213 where  $\text{true}_i$  is the true value in the *i*th province or AMS;  $\text{est}_i$  is the corresponding estimated value;  
 214  $\overline{\text{est}}$  and  $\overline{\text{true}}$  denote the mean of the estimated and true values, respectively; *N* is the number of  
 215 provinces or AMSs.

216

217 Additionally, in order to investigate the historical shifts of rice phenological dates in China, we  
 218 analyzed the trends of rice planting, heading, and maturity dates at the county level by a  
 219 Sen+Mann-Kendall trend analysis at a significance level of 0.05. The trend analysis method is detailed  
 220 in Gocic et al. (2013).

## 221 3 Result

### 222 3.1 Validation of ChinaRiceCalendar

223 The key phenological dates estimated in the study show high consistency with the data from AMSs  
 224 (Fig. 3). The R<sup>2</sup> between rice phenological dates from ChinaRiceCalendar and AMSs is 0.95. The R<sup>2</sup>  
 225 between ChinaRiceCalendar and AMS data for transplanting, heading, and maturity dates in China is  
 226 0.91, 0.88, and 0.90, respectively. The RMSEs of transplanting, heading, and maturity dates in  
 227 ChinaRiceCalendar are approximately 14 days. The R<sup>2</sup> between rice phenological dates from

228 ChinaRiceCalendar and AMS data for early, middle, and late rice is 0.91, 0.94 and 0.90, respectively.

229

230 Also, we calculated the RMSE of the estimated rice cropping dates in the seven agricultural regions in  
231 China (Fig. 4). Overall, the estimated rice calendars are more accurate in northern China than in the  
232 south. For early-season rice, the RMSE average of the estimated cropping dates is 12.73, 12.43, and  
233 14.53 days in the MLY, SC, and YGP, respectively. For middle-season rice, the range of the RMSEs in  
234 the seven agricultural regions is from 4.74 days in the HP to 14.34 days in the YGP. For late-season  
235 rice, the RMSE average of the estimated cropping dates is 13.90, 17.54, and 14.25 days in the MLY,  
236 SC, and YGP, respectively.

### 237 **3.2 Comparison with other calendar datasets**

238 Using AMS field observations as benchmarks, the RMSE of rice phenological dates obtained from  
239 ChinaRiceCalendar, ChinaCropPhen1km, RiceAtlas, and RICA is 13.8 days, 15.0 days, 17.9 days, and  
240 22.6 days, respectively. According to the accuracy evaluation at the seasonal level (Fig. 5),  
241 ChinaRiceCalendar is the only dataset where the RMSE does not exceed 15 days across three rice  
242 seasons. Compared with the ChinaRiceCalendar dataset, ChinaCropPhen1km exhibits suboptimal  
243 performance in early-rice seasons (RMSE=18days), RiceAtlas underperforms in middle-rice seasons  
244 (RMSE=22days), and RICA falls short in both middle- and late-rice seasons (RMSE>30days). Overall,  
245 ChinaRiceCalendar demonstrates superior accuracy in the estimated rice calendars compared to  
246 ChinaCropPhen1km, RiceAtlas, and RICA at the annual and seasonal levels in China.

### 247 **3.3 Spatial distribution of rice phenological dates**

248 According to the spatial distribution of the detected rice areas during 2003~2022, early and late rice  
249 were mainly grown in southern China, while middle rice was widely planted in China from south to  
250 north (Figs. 6 and 7). The spatial variations of rice phenology were significant in early, middle, and late  
251 seasons. In the NP, HP, and LP, middle rice was transplanted around DOY150, flowered around  
252 DOY230, and matured around DOY270. In the YGP, the mean transplanting date was approximately  
253 DOY100 for early rice, DOY150 for middle rice, and DOY195 for late rice; the mean heading date for  
254 early, middle, and late rice was DOY170, DOY230, and DOY250, respectively; the mean maturity date  
255 was approximately DOY200 for early rice, DOY260 for middle rice, and DOY290 for late rice. In the  
256 MLY, the mean transplanting date was approximately DOY120 for early rice, DOY160 for middle rice,  
257 and DOY200 for late rice; the mean heading date was approximately DOY190 for early rice, DOY230  
258 for middle rice, and DOY250 for late rice; the mean maturity date was DOY210 for early rice,  
259 DOY260 for middle rice, and DOY290 for late rice. In the SC, the mean transplanting date was  
260 approximately DOY100 for early rice and DOY220 for late rice; the mean heading date was  
261 approximately DOY170 for early rice and DOY270 for late rice; the mean maturity date was  
262 approximately DOY200 for early rice and DOY300 for late rice. For rice in the SCS, the mean  
263 transplanting, heading, and maturity dates were approximately DOY130, DOY220, and DOY250,  
264 respectively.

### 265 **3.4 Temporal changes in rice phenological dates**

266 Based on the trend analysis of rice phenological dates from 2003 to 2022 in China (Fig. 8), the mean  
267 transplanting dates for early, middle, and late rice shifted by +0.74, -0.68, and -5.12 DOY/decade,

268 respectively; the mean heading dates for early, middle, and late rice shifted by -0.51, +2.73, and -0.60  
269 DOY/decade, respectively; the mean maturity dates for early, middle, and late rice shifted by -0.67,  
270 +3.75, and -1.62 DOY/decade, respectively. The detected shifts in rice phenological dates during  
271 2003~2022 depended on the agricultural region (Fig. 9). For middle-season rice in the Northeast Plain  
272 (NP), 76% of the counties showed a significant or slight advance in transplanting dates, while 71% of  
273 the counties showed a significant or slight delay in maturity dates. In the Middle and Lower Yangtze  
274 River Region (MLY), 59%, 66%, and 72% of the rice-producing counties showed a significant or slight  
275 delay in transplanting, heading, and maturity dates of middle rice, respectively. In the Sichuan Basin  
276 and Surrounding Region (SCS), 79%, 86%, and 80% of the rice-producing counties showed a  
277 significant or slight delay in transplanting, heading, and maturity dates of middle rice, respectively. In  
278 the Yunnan-Guizhou Plateau (YGP), 77%, 67%, and 59% of the rice-producing counties showed a  
279 significant or slight delay in transplanting, heading, and maturity dates of middle rice, respectively. In  
280 the Huanghuaihai Plain (HP) and the Loess Plateau (LP), rice phenological dates did not show a  
281 consistent or significant trend. For early-season rice, transplanting tends to be delayed, but maturity  
282 tends to be earlier in the Southern China Region (SC). In most parts of China, the detected trends in  
283 early rice phenological dates were not significant during 2003~2022. For late-season rice in China,  
284 64% of the counties showed a significant or slight advance in transplanting dates, whereas 64% of the  
285 counties showed a significant or slight delay in heading and maturity dates.

## 286 **4 Uncertainties in ChinaRiceCalendar**

287 This study used MODIS remote sensing data to extract rice phenological dates in various growing  
288 seasons in China. The MODIS remote sensing products have an appropriate temporal resolution, long  
289 time series, and good time consistency for analyzing changes in rice calendars at the regional scale.  
290 Moreover, the MODIS data are easy to obtain and process on the GEE platform, allowing for  
291 automated and timely updating of the calendar dataset. Nevertheless, discerning early- and late-rice  
292 pixels is more difficult than identifying middle-rice pixels in MODIS data, resulting in lower accuracy  
293 of the detected rice calendars in southern China (MLY, SC, SCS, YGP) than in northern China (NP,  
294 HP, LP).

295  
296 There are several factors leading to the incomplete identification of rice pixels in early and late seasons  
297 in southern China. Firstly, the pixel-based detection of rice areas may be interfered with by the  
298 contamination of clouds, aerosols, and water vapor, especially during the monsoon season when late  
299 rice is transplanted (Xiao et al., 2005; Xiao et al., 2014; Clauss et al., 2016; Mishra et al., 2021).  
300 Because synthetic aperture radar (SAR) can penetrate through clouds, subsequent studies could  
301 combine optical and SAR images to avoid the impacts of clouds (Shen et al., 2023a). Utilizing  
302 geostationary satellite observations to increase the temporal frequency of remote sensing data may also  
303 be an effective way to improve accuracy of rice calendars (Shen et al., 2023b). Secondly, diverse  
304 multi-cropping systems, complex topography, and the fragmentation of croplands in southern China  
305 make the pixel detection for early and late rice more challenging (Dong and Xiao, 2016). Producing  
306 satellite remote sensing data with higher spatial resolution and integrating multiple data sources from  
307 satellite-airborne-ground observations will facilitate real-time monitoring of rice cropping areas at the  
308 regional scale (Zheng et al., 2022; Sun et al., 2023). Additionally, the PhenoRice algorithm falls short  
309 in detecting rice pixels in rainfed or upland rice systems due to the absence of clear agronomic flooding



310 signals. In China, rice is mainly planted in flooded paddy fields (Luo et al., 2022), which mitigates the  
311 problems of detecting rainfed or upland rice. Last but not least, precisely corresponding the image  
312 pixels from the MODIS dataset to the Agricultural Meteorological Stations remains a challenge during  
313 data validation. In the future, it would be beneficial to conduct a quantitative assessment to determine  
314 the representativeness of the MODIS pixels surrounding the AMS site.

315  
316 In this study, we improved the method of growing season division in the PhenoRice algorithm. We also  
317 attempted to remove non-paddy pixels and reduce the impacts of low-quality data on the reconstruction  
318 of EVI time-series curves. Although the local tuning of the PhenoRice algorithm parameters could  
319 further improve the results, we employed a single configuration of EVI threshold values ( $EVI_{max\_th}$ ,  
320  $EVI_{min\_th}$ ,  $Wind_{ecr}$ , and  $dec_{th}$ ) in the PhenoRice algorithm across China because automated methods that  
321 perform robustly are essential for developing timely information about crop calendars over large  
322 extents (Mishra et al., 2021). Subsequently, we will try to automate the generation and updating of  
323 ChinaRiceCalendar based on the ‘rgee’ package (Aybar et al., 2023).

## 324 5 Data Availability

325 ChinaRiceCalendar is a raster dataset with 1-km spatial resolution. The dataset falls into two parts:  
326 detected rice pixel data (\*\_rice\_pixels.tif) and county-level rice calendar data (\*\_county\_level.tif). The  
327 spatial reference system of the dataset is WGS\_1984\_UTM\_Zone\_49N. The dataset currently includes  
328 mean calendar dates during five periods: 2003~2007, 2008~2012, 2013~2017, 2018~2022, and  
329 2003~2022. ChinaRiceCalendar is available at <https://doi.org/10.7910/DVN/EUP8EY> (Liu et al.,  
330 2023).

## 331 6 Conclusions

332 Utilizing MODIS time series data, we established a multi-season rice calendar dataset named  
333 ChinaRiceCalendar, encompassing transplanting, heading, and maturity dates of early, middle, and late  
334 rice in China from 2003 to 2022. The rice phenological dates within ChinaRiceCalendar, estimated  
335 through the enhanced PhenoRice algorithm, exhibit strong alignment with field observations collected  
336 by Agricultural Meteorological Stations across China. The  $R^2$  values between ChinaRiceCalendar and  
337 field data for early, middle, and late rice consistently surpass 0.90, with RMSE values below 15 days in  
338 three rice seasons. According to the calendar data from 2003 to 2022, the transplanting dates for early,  
339 middle, and late rice shifted by +0.7, -0.7, and -5.1 DOY/decade, respectively; the heading date for  
340 early, middle, and late rice shifted by -0.5, +2.7, and -0.6 DOY/decade, respectively; the maturity date  
341 for early, middle, and late rice shifted by -0.7, +3.8, and -1.6 DOY/decade, respectively. In summary,  
342 ChinaRiceCalendar stands as a reliable dataset for investigating and optimizing the spatio-temporal  
343 dynamics of rice cultivation in China, particularly in the context of climate and land-use changes.

344 **Author Contribution:** Conceptualization and methodological, HL and XW; algorithmic  
345 improvements, HL; data download and processing, JL, YL and ZL; validation, JL, SC and QW; formal  
346 analysis, HL, XW, and TZ; writing-original draft preparation, HL and XW; writing-review and editing,  
347 XW, SW and LW. All authors have read and agreed to the published version of the manuscript.

348

349 **Financial support:** This research has been supported by the National Natural Science Foundation of  
350 China (Project Nos. 31861143015 and 32301393).

351

352 **Acknowledgments:** We would like to thank Dongdong Kong from China University of Geosciences  
353 (Wuhan) for providing the R package *Phnofit* and thank Mirco Boschetti from the Italian National  
354 Research Council for providing the source code of *PhenoRice*.

355

356 **Competing interests:** The contact author has declared that none of the authors has any competing  
357 interests.

## 358 **References**

359 Atzberger, C. and Eilers, P.H.: Evaluating the effectiveness of smoothing algorithms in the absence of  
360 ground reference measurements. *International Journal of Remote Sensing*, 32(13), 3689-3709, 2011.

361 Aybar, C. rgee: R Bindings for Calling the 'Earth Engine' API (Version 1.1.7).  
362 <https://github.com/r-spatial/rgee/issues/>, 2023.

363 Bai, H. and Xiao, D.: Spatiotemporal changes of rice phenology in China during 1981 – 2010.  
364 *Theoretical and Applied Climatology*, 140, 1483-1494, 2020.

365 Boschetti, M., Busetto, L., Manfron, G., Laborte, A., Asilo, S., Pazhanivelan, S. and Nelson, A.:  
366 PhenoRice: A method for automatic extraction of spatio-temporal information on rice crops using  
367 satellite data time series. *Remote sensing of environment*, 194, 347-365, 2017.

368 Boschetti, M., Stroppiana, D., Brivio, P. and Bocchi, S.: Multi-year monitoring of rice crop phenology  
369 through time series analysis of MODIS images. *International journal of remote sensing*, 30(18),  
370 4643-4662, 2009.

371 Busetto, L., Zwart, S.J. and Boschetti, M.: Analysing spatial – temporal changes in rice cultivation  
372 practices in the Senegal River Valley using MODIS time-series and the PhenoRice algorithm.  
373 *International Journal of Applied Earth Observation and Geoinformation*, 75, 15-28, 2019.

374 Bush, E.R., Abernethy, K.A., Jeffery, K., Tutin, C., White, L., Dimoto, E., Dikangadissi, J.T., Jump,  
375 A.S. and Bunnefeld, N.: Fourier analysis to detect phenological cycles using long - term tropical field  
376 data and simulations. *Methods in Ecology and Evolution*, 8(5), 530-540, 2017.

377 Cao, J., Cai, X., Tan, J., Cui, Y., Xie, H., Liu, F., Yang, L. and Luo, Y.: Mapping paddy rice using  
378 Landsat time series data in the Ganfu Plain irrigation system, Southern China, from 1988 – 2017.  
379 *International Journal of Remote Sensing*, 42(4), 1556-1576, 2021.

380 Carleton, T.A.: Crop-damaging temperatures increase suicide rates in India. *Proceedings of the*  
381 *National Academy of Sciences*, 114(33), 8746-8751, 2017.

382 Clauss, K., Yan, H. and Kuenzer, C.: Mapping paddy rice in China in 2002, 2005, 2010 and 2014 with  
383 MODIS time series. *Remote Sensing*, 8(5), 434, 2016.

384 Dong, J. and Xiao, X.: Evolution of regional to global paddy rice mapping methods: A review. *ISPRS*

385 Journal of Photogrammetry and Remote Sensing, 119, 214-227, 2016.

386 Fahad, S., Adnan, M., Noor, M., Arif, M., Alam, M., Khan, I.A., Ullah, H., Wahid, F., Mian, I.A. and  
387 Jamal, Y.: Major constraints for global rice production, *Advances in rice research for abiotic stress*  
388 *tolerance*. Elsevier, pp. 1-22, 2019.

389 Franke, J.A., Müller, C., Elliott, J., Ruane, A.C., Jägermeyr, J., Snyder, A., Dury, M., Falloon, P.D.,  
390 Folberth, C. and François, L.: The GGCM Phase 2 emulators: global gridded crop model responses to  
391 changes in CO<sub>2</sub>, temperature, water, and nitrogen (version 1.0). *Geoscientific Model Development*,  
392 13(9), 3995-4018, 2020.

393 Fritz, S., See, L., Bayas, J.C.L., Waldner, F., Jacques, D., Becker-Reshef, I., Whitcraft, A., Baruth, B.,  
394 Bonifacio, R. and Crutchfield, J.: A comparison of global agricultural monitoring systems and current  
395 gaps. *Agricultural systems*, 168, 258-272, 2019.

396 Frolking, S., Qiu, J., Boles, S., Xiao, X., Liu, J., Zhuang, Y., Li, C. and Qin, X.: Combining remote  
397 sensing and ground census data to develop new maps of the distribution of rice agriculture in China.  
398 *Global Biogeochemical Cycles*, 16(4), 38-1-38-10, 2002.

399 Gao, F. and Zhang, X.: Mapping crop phenology in near real-time using satellite remote sensing:  
400 Challenges and opportunities. *Journal of Remote Sensing*, 2021, 2021.

401 Gocic, M. and Trajkovic, S.: Analysis of changes in meteorological variables using Mann-Kendall and  
402 Sen's slope estimator statistical tests in Serbia. *Global and Planetary Change*, 100, 172-182, 2013.

403 Gumma, M.K., Nelson, A., Thenkabail, P.S. and Singh, A.N.: Mapping rice areas of South Asia using  
404 MODIS multitemporal data. *Journal of applied remote sensing*, 5(1), 053547, 2011.

405 Guo, L., An, N. and Wang, K.: Reconciling the discrepancy in ground- and satellite-observed trends in  
406 the spring phenology of winter wheat in China from 1993 to 2008. *Journal of Geophysical Research:*  
407 *Atmospheres*, 121(3), 1027-1042, 2016.

408 Han, J., Zhang, Z., Luo, Y., Cao, J., Zhang, L., Zhuang, H., Cheng, F., Zhang, J. and Tao, F.: Annual  
409 paddy rice planting area and cropping intensity datasets and their dynamics in the Asian monsoon  
410 region from 2000 to 2020. *Agricultural Systems*, 200, 103437, 2022.

411 He, Y., Dong, J., Liao, X., Sun, L., Wang, Z., You, N., Li, Z. and Fu, P.: Examining rice distribution and  
412 cropping intensity in a mixed single- and double-cropping region in South China using all available  
413 Sentinel 1/2 images. *International Journal of Applied Earth Observation and Geoinformation*, 101,  
414 102351, 2021.

415 Liu, J., Li, H., Wang, X., Wang, S., Liu, Y., Liu, Z., Chen, S., Wang Q., Zhu, T., Wang, L., Wang, L.:  
416 *ChinaRiceCalendar*. Harvard Dataverse, doi/10.7910/DVN/EUP8EY, 2023.

417 IPCC. Climate change 2022: impacts, adaptation and vulnerability.  
418 <https://www.ipcc.ch/report/sixth-assessment-report-working-group-ii/>, 2022.

419 Kim, D.-H., Jang, T., Hwang, S., and Jeong, H.: Paddy rice adaptation strategies to climate change:  
420 Transplanting date shift and BMP applications, *Agricultural Water Management*, 252, 106926, 2021.

421 Kong, D., McVicar, T.R., Xiao, M., Zhang, Y., Peña - Arancibia, J.L., Filippa, G., Xie, Y. and Gu, X.:

422 phenofit: An R package for extracting vegetation phenology from time series remote sensing. *Methods*  
423 *in Ecology and Evolution*, 2022.

424 Kotsuki, S. and Tanaka, K.: SACRA – a method for the estimation of global high-resolution crop  
425 calendars from a satellite-sensed NDVI. *Hydrology and Earth System Sciences*, 19(11), 4441-4461,  
426 2015.

427 Laborte, A.G., Gutierrez, M.A., Balanza, J.G., Saito, K., Zwart, S.J., Boschetti, M., Murty, M., Villano,  
428 L., Aunario, J.K. and Reinke, R.: RiceAtlas, a spatial database of global rice calendars and production.  
429 *Scientific data*, 4(1), 1-10, 2017.

430 Liu, L., Huang, J., Xiong, Q., Zhang, H., Song, P., Huang, Y., Dou, Y. and Wang, X.: Optimal MODIS  
431 data processing for accurate multi-year paddy rice area mapping in China. *GIScience & Remote*  
432 *Sensing*, 57(5), 687-703, 2020.

433 Liu, Y., Zhou, W. and Ge, Q.: Spatiotemporal changes of rice phenology in China under climate change  
434 from 1981 to 2010. *Climatic Change*, 157, 261-277, 2019.

435 Luo, W., Chen, M., Kang, Y., Li, W., Li, D., Cui, Y., Khan, S. and Luo, Y.: Analysis of crop water  
436 requirements and irrigation demands for rice: Implications for increasing effective rainfall. *Agricultural*  
437 *Water Management*, 260, 107285, 2022.

438 Luo, Y., Zhang, Z., Chen, Y., Li, Z. and Tao, F.: ChinaCropPhen1km: a high-resolution crop  
439 phenological dataset for three staple crops in China during 2000–2015 based on leaf area index (LAI)  
440 products. *Earth System Science Data*, 12(1), 197-214, 2020.

441 Mishra, B., Busetto, L., Boschetti, M., Laborte, A. and Nelson, A.: RICA: A rice crop calendar for Asia  
442 based on MODIS multi year data. *International Journal of Applied Earth Observation and*  
443 *Geoinformation*, 103, 102471, 2021.

444 More, R.S., Manjunath, K., Jain, N.K., Panigrahy, S. and Parihar, J.S.: Derivation of rice crop calendar  
445 and evaluation of crop phenometrics and latitudinal relationship for major south and south-east Asian  
446 countries: A remote sensing approach. *Computers and Electronics in Agriculture*, 127, 336-350, 2016.

447 Nelson, A. and Gumma, M.: A map of lowland rice extent in the major rice growing countries of Asia.  
448 IRRI, Los Banos, Philippines, 2015.

449 Pan, Z., Huang, J., Zhou, Q., Wang, L., Cheng, Y., Zhang, H., Blackburn, G.A., Yan, J. and Liu, J.:  
450 Mapping crop phenology using NDVI time-series derived from HJ-1 A/B data. *International Journal of*  
451 *Applied Earth Observation and Geoinformation*, 34, 188-197, 2015.

452 Parmesan, C., Morecroft, M.D. and Trisurat, Y.: *Climate change 2022: Impacts, adaptation and*  
453 *vulnerability*, GIEC, 2022.

454 Qiu, J., Tang, H., Froking, S., Boles, S., Li, C., Xiao, X., Liu, J., Zhuang, Y. and Qin, X.: Mapping  
455 single-, double-, and triple-crop agriculture in China at 0.5°× 0.5° by combining county-scale census  
456 data with a remote sensing-derived land cover map. *Geocarto International*, 18(2), 3-13, 2003.

457 Reed, B.C., Brown, J.F., VanderZee, D., Loveland, T.R., Merchant, J.W. and Ohlen, D.O.: Measuring  
458 phenological variability from satellite imagery. *Journal of vegetation science*, 5(5), 703-714, 1994.

459 Sakamoto, T., Wardlow, B.D., Gitelson, A.A., Verma, S.B., Suyker, A.E. and Arkebauer, T.J.: A  
460 two-step filtering approach for detecting maize and soybean phenology with time-series MODIS data.  
461 *Remote Sensing of Environment*, 114(10), 2146-2159, 2010.

462 Sakamoto, T., Yokozawa, M., Toritani, H., Shibayama, M., Ishitsuka, N. and Ohno, H.: A crop  
463 phenology detection method using time-series MODIS data. *Remote sensing of environment*, 96(3-4),  
464 366-374, 2005.

465 Sakamoto, T.: Refined shape model fitting methods for detecting various types of phenological  
466 information on major US crops. *ISPRS Journal of Photogrammetry and Remote Sensing*, 138, 176-192,  
467 2018.

468 Shen, R., Pan, B., Peng, Q., Dong, J., Chen, X., Zhang, X., Ye, T., Huang, J. and Yuan, W.:  
469 High-resolution distribution maps of single-season rice in China from 2017 to 2022. *Earth System  
470 Science Data Discussions*, 1-27, 2023a.

471 Shen, Y., Zhang, X., Yang, Z., Ye, Y., Wang, J., Gao, S., Liu, Y., Wang, W., Tran, K.H. and Ju, J.:  
472 Developing an operational algorithm for near-real-time monitoring of crop progress at field scales by  
473 fusing harmonized Landsat and Sentinel-2 time series with geostationary satellite observations. *Remote  
474 Sensing of Environment*, 296, 113729, 2023b.

475 Shihua, L., Jingtao, X., Ping, N., Jing, Z., Hongshu, W. and Jingxian, W.: Monitoring paddy rice  
476 phenology using time series MODIS data over Jiangxi Province, China. *International Journal of  
477 Agricultural and Biological Engineering*, 7(6), 28-36, 2014.

478 Son, N.-T., Chen, C.-F., Chen, C.-R., Duc, H.-N. and Chang, L.-Y.: A phenology-based classification of  
479 time-series MODIS data for rice crop monitoring in Mekong Delta, Vietnam. *Remote Sensing*, 6(1),  
480 135-156, 2013.

481 Sun, C., Zhang, H., Xu, L., Ge, J., Jiang, J., Zuo, L. and Wang, C.: Twenty-meter annual paddy rice  
482 area map for mainland Southeast Asia using Sentinel-1 synthetic-aperture-radar data. *Earth System  
483 Science Data*, 15(4), 1501-1520, 2023.

484 Sun, H., Huang, J. and Peng, D.: Detecting major growth stages of paddy rice using MODIS data. *J.  
485 Remote Sens*, 13, 1122-1137, 2009.

486 Waha, K., Müller, C. and Rolinski, S.: Separate and combined effects of temperature and precipitation  
487 change on maize yields in sub-Saharan Africa for mid-to late-21st century. *Global and Planetary  
488 Change*, 106, 1-12, 2013.

489 Wang, J., Yu, K., Tian, M. and Wang, Z.: Estimation of rice key phenology date using Chinese HJ-1  
490 vegetation index time-series images, 2019 8th International Conference on Agro-Geoinformatics  
491 (Agro-Geoinformatics). IEEE, pp. 1-4, 2019.

492 Wang, X., Ciais, P., Li, L., Ruget, F., Vuichard, N., Viovy, N., Zhou, F., Chang, J., Wu, X. and Zhao, H.:  
493 Management outweighs climate change on affecting length of rice growing period for early rice and  
494 single rice in China during 1991–2012. *Agricultural and Forest Meteorology*, 233, 1-11, 2017.

495 Wang, X., Folberth, C., Skalsky, R., Wang, S., Chen, B., Liu, Y., Chen, J. and Balkovic, J.: Crop  
496 calendar optimization for climate change adaptation in rice-based multiple cropping systems of India

497 and Bangladesh. *Agricultural and Forest Meteorology*, 315, 108830, 2022.

498 Wang, X., Wang, S., Folberth, C., Skalsky, R., Li, H., Liu, Y. and Balkovic, J.: Limiting global  
499 warming to 2 ° C benefits building climate resilience in rice-wheat systems in India through crop  
500 calendar management. *Agricultural Systems*, 213, 103806, 2024.

501 Wu, Q.: geemap: A Python package for interactive mapping with Google Earth Engine. *Journal of*  
502 *Open Source Software*, 5(51), 2305, 2020.

503 Xiao, X., Boles, S., Frohking, S., Li, C., Babu, J.Y., Salas, W. and Moore III, B.: Mapping paddy rice  
504 agriculture in South and Southeast Asia using multi-temporal MODIS images. *Remote sensing of*  
505 *Environment*, 100(1), 95-113, 2006.

506 Xiao, X., Boles, S., Liu, J., Zhuang, D., Frohking, S., Li, C., Salas, W. and Moore III, B.: Mapping  
507 paddy rice agriculture in southern China using multi-temporal MODIS images. *Remote sensing of*  
508 *environment*, 95(4), 480-492, 2005.

509 Zeng, L., Wardlow, B.D., Wang, R., Shan, J., Tadesse, T., Hayes, M.J. and Li, D.: A hybrid approach for  
510 detecting corn and soybean phenology with time-series MODIS data. *Remote Sensing of Environment*,  
511 181, 237-250, 2016.

512 Zhang, X., Friedl, M.A., Schaaf, C.B., Strahler, A.H., Hodges, J.C., Gao, F., Reed, B.C. and Huete, A.:  
513 Monitoring vegetation phenology using MODIS. *Remote sensing of environment*, 84(3), 471-475,  
514 2003.

515 Zhang, Z., Song, X., Tao, F., Zhang, S. and Shi, W.: Climate trends and crop production in China at  
516 county scale, 1980 to 2008. *Theoretical and Applied Climatology*, 123(1), 291-302, 2016.

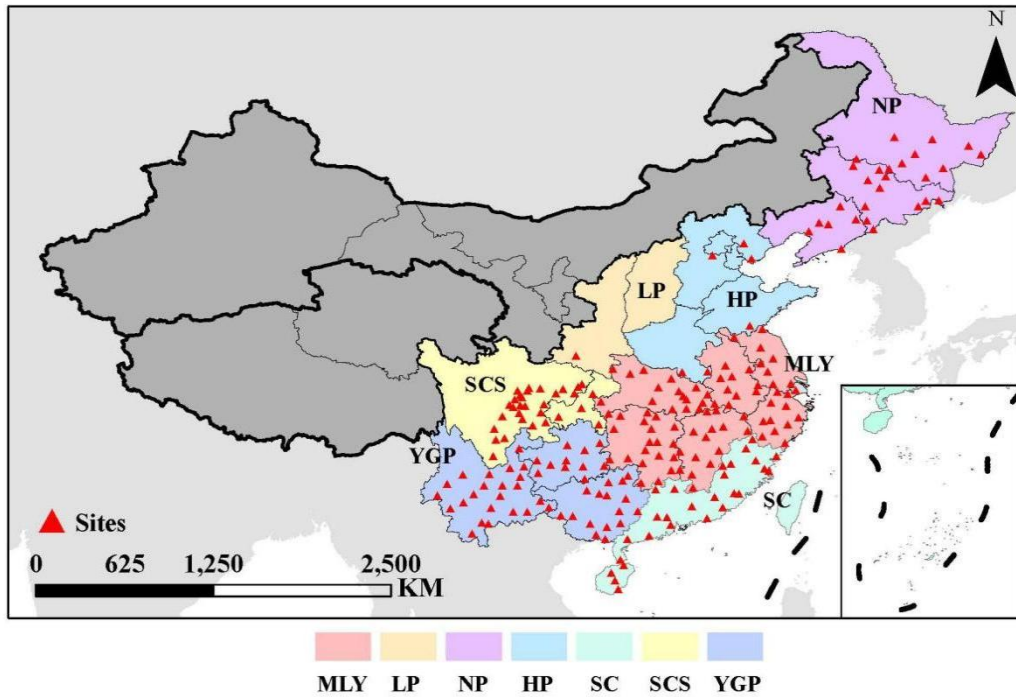
517 Zhao, C., Liu, B., Piao, S., Wang, X., Lobell, D.B., Huang, Y., Huang, M., Yao, Y., Bassu, S. and Ciais,  
518 P.: Temperature increase reduces global yields of major crops in four independent estimates.  
519 *Proceedings of the National Academy of sciences*, 114(35), 9326-9331, 2017.

520 Zhao, H., Yang, Z., Di, L. and Pei, Z.: Evaluation of temporal resolution effect in remote sensing based  
521 crop phenology detection studies, *International Conference on Computer and Computing Technologies*  
522 *in Agriculture*. Springer, pp. 135-150, 2011.

523 Zheng, J., Song, X., Yang, G., Du, X., Mei, X. and Yang, X.: Remote sensing monitoring of rice and  
524 wheat canopy nitrogen: A review. *Remote Sensing*, 14(22), 5712, 2022.

525 Zong, W., Ren, D., Huang, M., Sun, K., Feng, J., Zhao, J., Xiao, D., Xie, W., Liu, S. and Zhang,  
526 H.: Strong photoperiod sensitivity is controlled by cooperation and competition among Hd1, Ghd7  
527 and DTH8 in rice heading. *New Phytologist*, 229(3), 1635-1649, 2021.

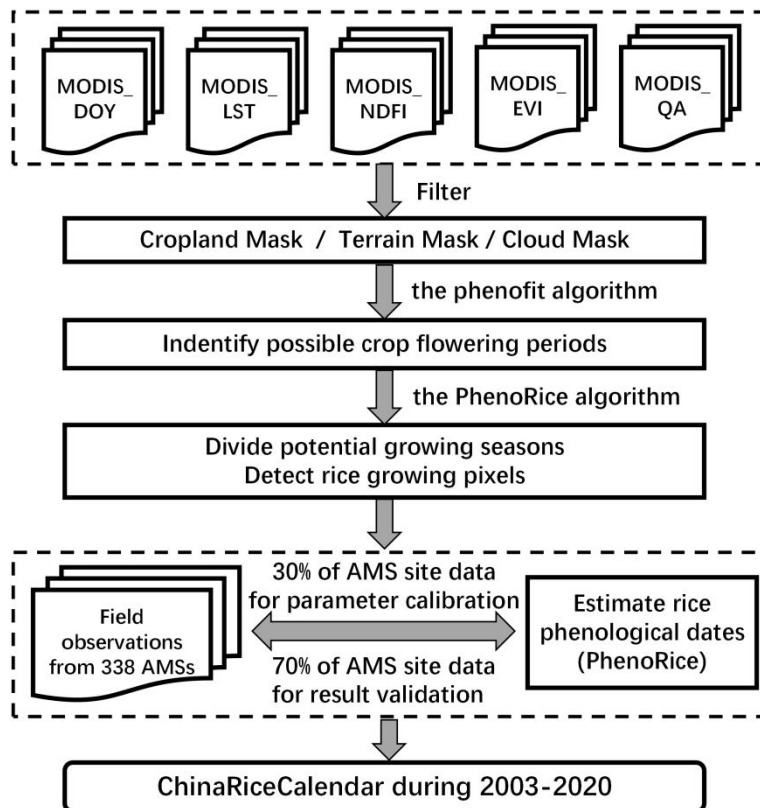
528



529

530

Fig. 1 Study area and distribution of Agricultural Meteorological Stations (AMSs) in China

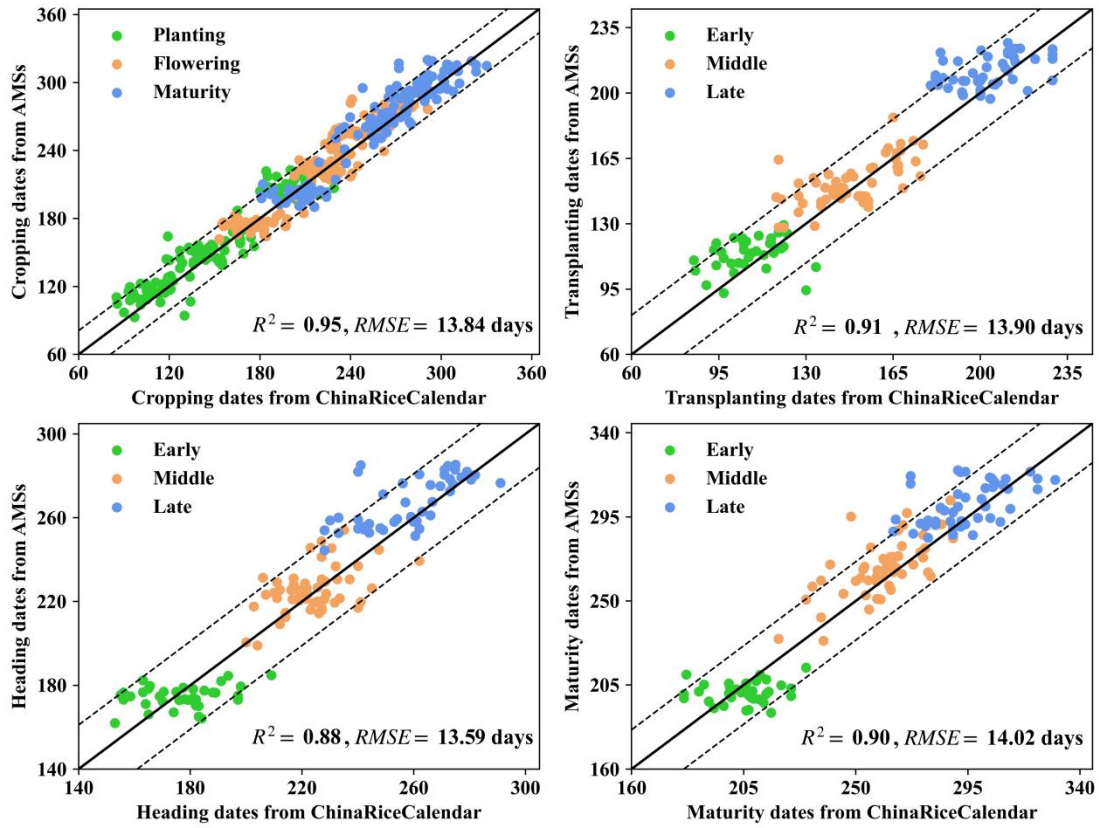


531

532

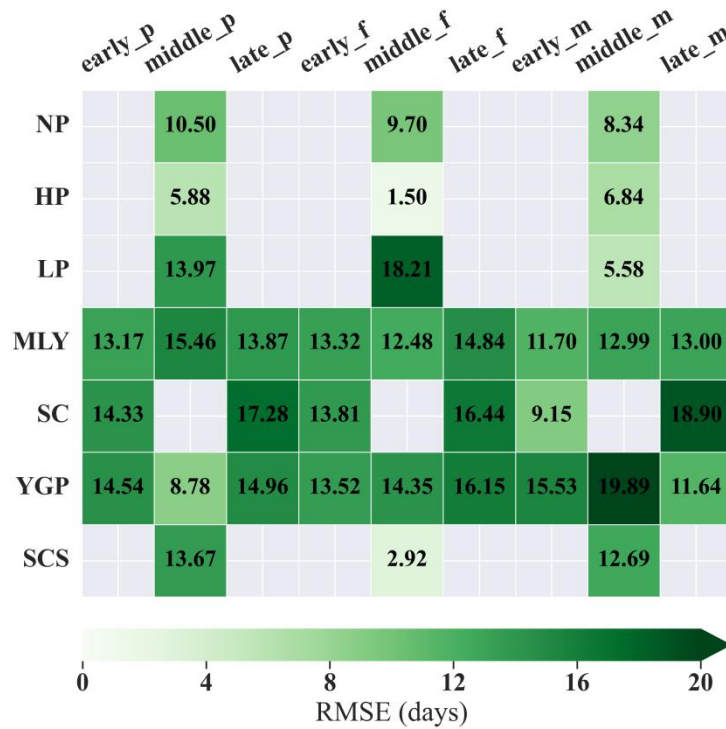
533

Fig. 2 Technology roadmap for this study



534

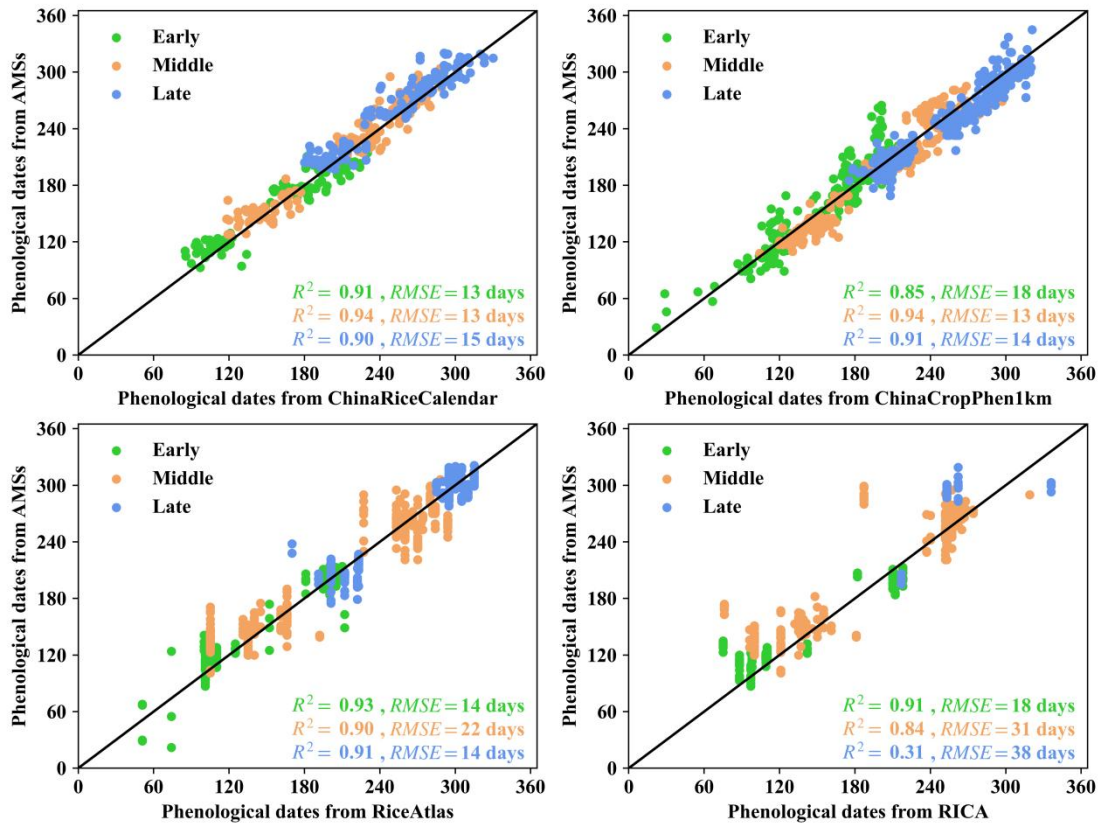
535 **Fig. 3 Comparison of rice phenological dates between ChinaRiceCalendar and AMS data at the**  
 536 **site scale (dashed lines are  $\pm 21$  days)**



537

538 **Fig. 4 RMSEs of rice phenological dates between ChinaRiceCalendar and AMS data in main**  
 539 **agricultural regions**



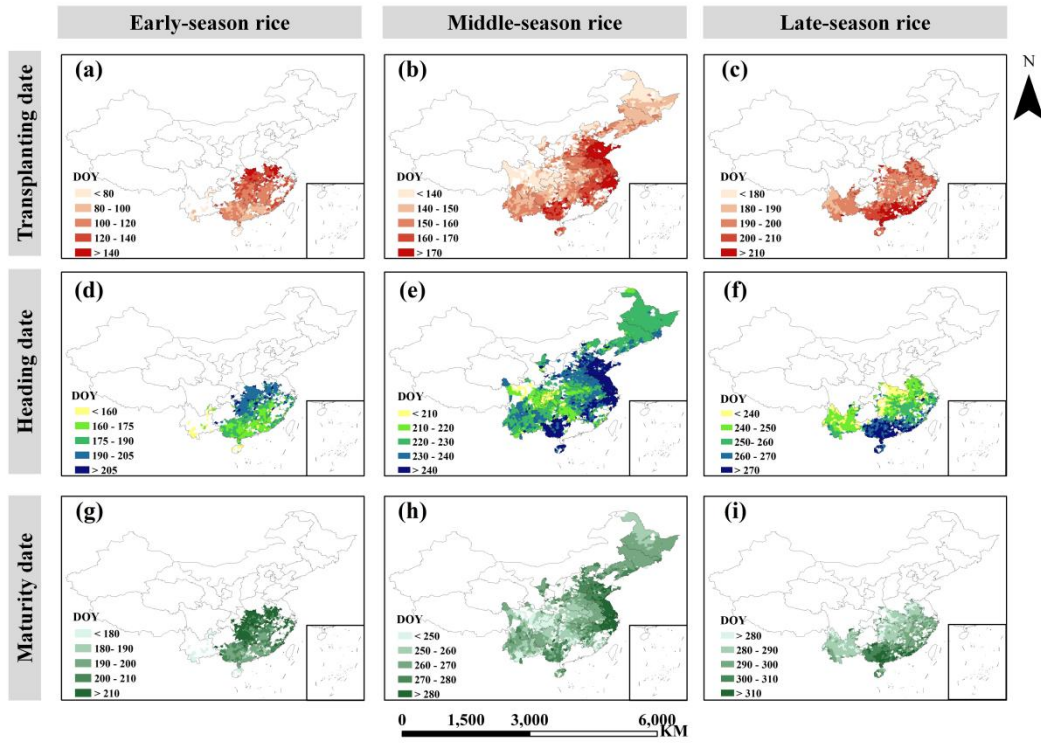


540

541 **Fig. 5 Comparison of rice phenological dates between calendar datasets and AMS data at the**  
 542 **site scale in early (green), middle (orange), and late (blue) seasons.**

543

544



545

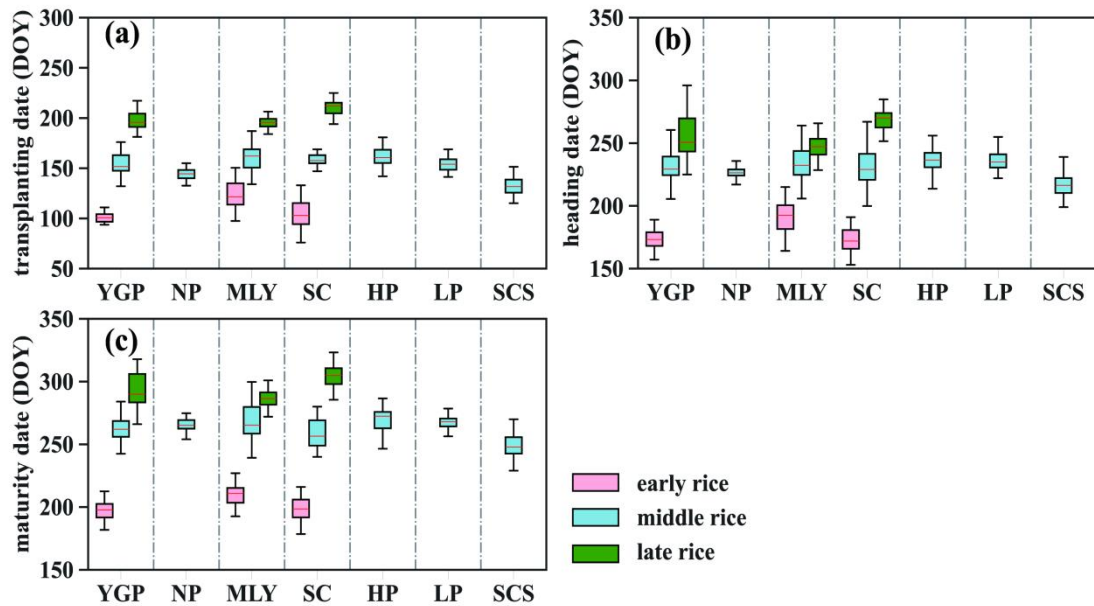
546

547

548

549

Fig. 6 Rice phenological dates at the county scale between 2003 and 2022 (a: early-rice transplanting dates; b: middle-rice transplanting dates; c: late-rice transplanting dates; d: early-rice heading dates; e: middle-rice heading dates; f: late-rice heading dates; g: early-rice maturity dates; h: middle-rice maturity dates; i: late-rice maturity dates)

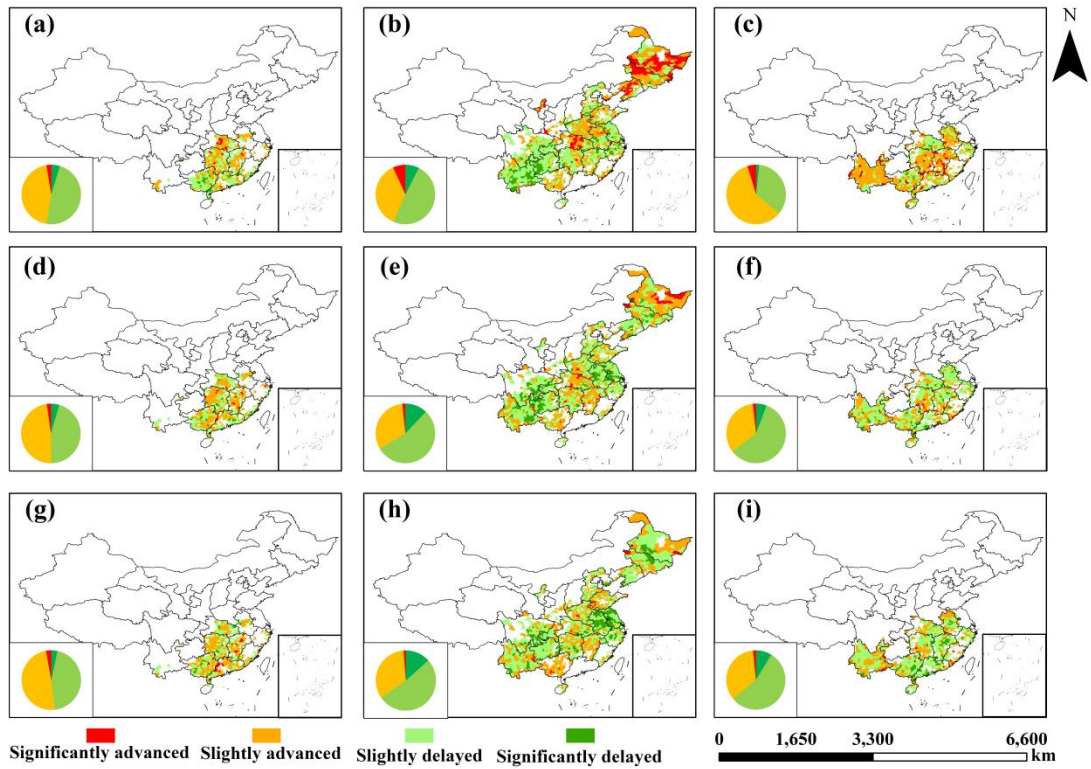


550

551

552

Fig. 7 Rice phenological dates in rice-producing counties between 2003 and 2022 (a: Transplanting dates; b: Heading dates; c: Maturity dates)



553

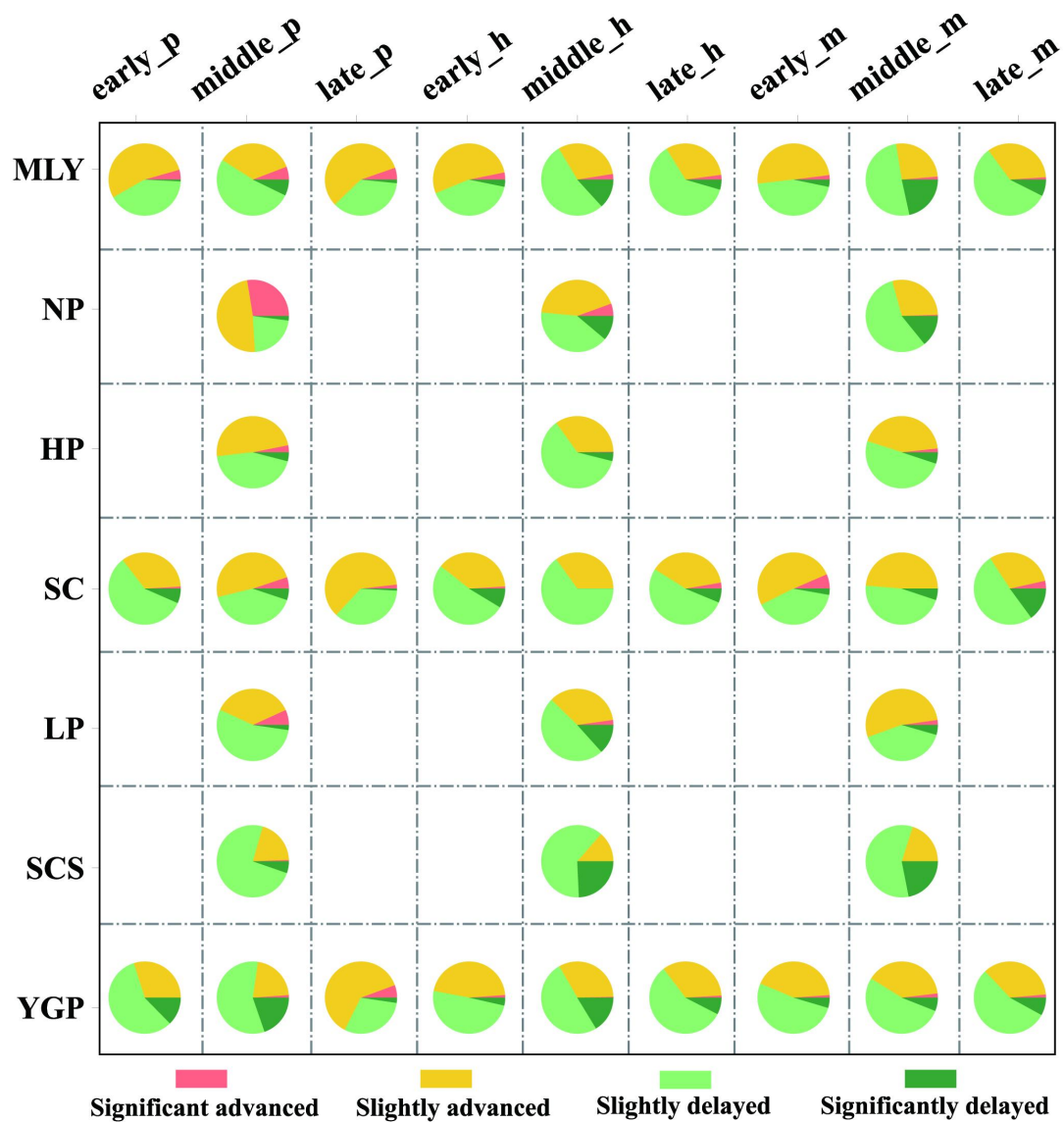
554

555

556

557

**Fig. 8** Temporal trends in rice phenological dates at the county scale from 2003 to 2022 (a: early-rice transplanting dates; b: middle-rice transplanting dates; c: late-rice transplanting dates; d: early-rice heading dates; e: middle-rice heading dates; f: late-rice heading dates; g: early-rice maturity dates; h: middle-rice maturity dates; i: late-rice maturity dates)



558

559 **Fig. 9** Temporal trends in rice phenological dates at the regional level from 2003 to 2022 (early\_p:  
 560 early-rice transplanting dates; middle\_p: middle-rice transplanting dates; late\_p: late-rice  
 561 transplanting dates; early\_h: early-rice heading dates; middle\_h: middle-rice heading dates;  
 562 late\_h: late-rice heading dates; early\_m: early-rice maturity dates; middle\_m: middle-rice  
 563 maturity dates; late\_m: late-rice maturity dates)

564 **Table 1 PhenoRice parameters used in the study** (EVI<sub>max\_th</sub>: EVI threshold above which a local  
565 maxima can be considered as a peak of a growing season; EVI<sub>min\_th</sub>: EVI threshold below which a  
566 local minima min can be considered as a start of a growing season; v11: shortest vegetative growth  
567 length; v12: longest vegetative growth length; t11: shortest field growth length; t12: longest field  
568 growth length; LST<sub>th</sub>: minimum land surface temperature for rice planting; Winfl: time window  
569 for capturing flooding signals; minndfi: threshold for NDFI; Wind<sub>decr</sub>: threshold for a decline  
570 window after EVI maximum; dec<sub>th</sub>: percent decrease of EVI after EVI maximum)

Province	EVI <sub>max_th</sub>	EVI <sub>min_th</sub>	v11 (days)	v12 (days)	t11 (days)	t12 (days)	LST <sub>th</sub> (°C)	Winfl (days)	minndfi	Wind <sub>decr</sub> (days)	Dec <sub>th</sub>
Anhui	0.4	0.25	32	72	64	120	15	24	0	64	0.5
Chongqing	0.4	0.25	64	88	96	136	15	24	0	64	0.5
Fujian	0.4	0.25	24	88	56	128	15	24	0	64	0.5
Guangdong	0.4	0.25	40	96	72	120	15	24	0	64	0.5
Guangxi	0.4	0.25	40	88	72	120	15	24	0	64	0.5
Guizhou	0.4	0.25	56	96	80	152	15	24	0	64	0.5
Hainan	0.4	0.25	56	112	80	128	15	24	0	64	0.5
Hebei	0.4	0.25	56	112	104	152	15	24	0	64	0.5
Heilongjiang	0.4	0.25	56	96	104	136	15	24	0	64	0.5
Henan	0.4	0.25	56	88	96	120	15	24	0	64	0.5
Hubei	0.4	0.25	24	112	56	152	15	24	0	64	0.5
Hunan	0.4	0.25	32	96	56	136	15	24	0	64	0.5
Jiangsu	0.4	0.25	56	88	104	136	15	24	0	64	0.5
Jiangxi	0.4	0.25	32	80	64	120	15	24	0	64	0.5
Jilin	0.4	0.25	56	96	96	136	15	24	0	64	0.5
Liaoning	0.4	0.25	56	96	104	152	15	24	0	64	0.5
Ningxia	0.4	0.25	64	88	112	152	15	24	0	64	0.5
Shaanxi	0.4	0.25	64	88	104	128	15	24	0	64	0.5
Shandong	0.4	0.25	56	80	96	120	15	24	0	64	0.5
Shanxi	0.4	0.25	64	88	104	128	15	24	0	64	0.5
Sichuan	0.4	0.25	56	96	80	160	15	24	0	64	0.5
Yunnan	0.4	0.25	24	112	56	160	15	24	0	64	0.5
Zhejiang	0.4	0.25	32	72	64	128	15	24	0	64	0.5

**Table 2** Classification criteria of seasons for detected rice calendars by province in China

Province	Early season		Middle season		Late season	
	Transplanting dates	Maturity dates	Transplanting dates	Maturity dates	Transplanting dates	Maturity dates
Anhui	110~150	190~220	130~180	240~280	190~230	270~320
Chongqing	--	--	110~160	210~280	--	--
Fujian	90~140	180~230	140~170	240~270	180~240	270~330
Guangdong	70~140	170~220	--	--	200~240	280~340
Guangxi	80~130	180~230	140~180	250~290	180~240	280~340
Guizhou	--	--	100~180	220~310	--	--
Hainan	10~80	110~190	140~180	240~280	180~220	280~320
Hebei	--	--	120~190	260~300	--	--
Heilongjiang	--	--	120~170	240~290	--	--
Henan	--	--	130~170	240~270	--	--
Hubei	110~160	170~220	110~180	230~280	180~220	270~330
Hunan	100~140	180~230	130~170	230~280	180~230	260~320
Jiangsu	--	--	150~190	260~310	--	--
Jiangxi	90~140	180~220	130~180	230~390	180~220	270~320
Jilin	--	--	130~170	240~280	--	--
Liaoning	--	--	130~170	260~290	--	--
Ningxia	--	--	120~160	250~290	--	--
Shaanxi	--	--	130~160	250~280	--	--
Shandong	--	--	170~200	270~300	--	--
Shanxi	--	--	140~170	250~280	--	--
Sichuan	--	--	100~170	210~300	--	--
Yunnan	10~90	130~180	90~170	210~310	170~230	260~330
Zhejiang	100~140	180~230	150~190	270~330	190~220	270~330